

Effects of particle angularity on granular self-organization

Dominik Krenzel* and Takashi Matsushima†

*Department of Engineering Mechanics and Energy, University of Tsukuba,
1-1-1, Tennodai, Tsukuba, 305-8573, Japan*

Haoran Jiang

*Civil Engineering Design Division, Kajima Corporation,
3-8-1, Motoakasaka, Minato-ku, Tokyo, 107-8477, Japan* ‡

Raphael Blumenfeld

Gonville & Caius College, University of Cambridge, UK §

(Dated: February 11, 2025)

Abstract

Recent studies of two-dimensional poly-disperse disc systems revealed a coordinated self-organisation of cell stresses and shapes, with certain distributions collapsing onto a master form for many processes, size distributions, friction coefficients, and cell orders. Here we examine the effects of grain angularity on the indicators of self-organisation, using simulations of bi-disperse regular N -polygons and varying N systematically. We find that: the strong correlation between local cell stresses and orientations, as well as the collapses of the conditional distributions of scaled cell stress ratios to a master Weibull form for all cell orders k , are independent of angularity and friction coefficient. In contrast, increasing angularity makes the collapses of the conditional distributions sensitive to changes in the friction coefficient.

* Krenzel.Dominik.kb@u.tsukuba.ac.jp

† tmatsu@kz.tsukuba.ac.jp

‡ jiangh@kajima.com

§ rbb11@cam.ac.uk; Also at Imperial College London, London SW7 2AZ, UK

I. INTRODUCTION

Understanding behaviour of granular matter is essential in many fields of research and technology. Macroscale models of stress transmission in such media involve upscaled constitutive properties that often presume independence of the stress field, which enables explicit solutions. The constitutive properties are sensitive to the local grain-scale structural characteristics, but these were shown recently to be strongly correlated with the local stress due to a cooperative local stress-structure self-organization [1–3]. Significantly, this calls into question models involving linear stress field equations. While relation between macroscopic properties and grain-scale characteristics, such as force-chains, have been studied extensively, advances on effects of dynamics on the settled structure have been limited [4–6]. Recent studies of planar (2D) disc packings have shown that the basic organizable structural elements, cells, which are the smallest voids surrounded by grains in contact, self-organize during slow dynamics in ways that transcend particular system and process details [1–3, 7, 8], including remarkable steady-state features [9–12].

These studies beg the obvious question how the self-organisation (SO) is affected by grain angularity. Not only are non-spherical grains more ubiquitous in nature but they also restrict mobility and affect differently the stability of granular aggregates. However, because of the involved analytical and numerical treatments of such shapes, a limited body of work exists on such systems, e.g. [13–16]. While the combined effects of grain shape and friction on bulk properties have received some attention [17–19], the micro-structural effects on cell characteristics in 2D are not fully understood, with work so far limited to squares with rounded corners [20].

A way to explore effects of particle angularity in 2D, while making connection with discs is by studying N -sided regular polygonal grains and varying N systematically. The polygons approach discs in the limit $N \rightarrow \infty$. Here, we investigate systematically which of the observed indicators of SO [3, 14, 21] survive the increasing angularity, as well as the interplay between angularity and friction.

II. NUMERICAL SIMULATIONS

A. Simulation setup

We performed isotropic biaxial compression tests on systems of regular convex N -polygons with $N = 5, 6, 13$, and 64 the number of polygon edges. In our simulations, we used the hard-particle soft-contact Discrete Element Method [14, 22]. In each simulation, 2200-2800 frictionless particles of equal shape were deposited under gravity to generate dense initial packings. To minimize crystallization, each assembly contained a mixture of 80% small and 20% large particles. Once generated, gravity was disabled and the systems were compressed uniaxially until the pressure on all four walls reached 20kPa. Energy was then allowed to dissipate until pressure fluctuations decayed to less than 10^{-14} of the constant pressure. At this 'initial' state, intergranular friction, μ , was switched on and the packing was compressed biaxially in the direction of gravity, keeping the side walls at constant pressure of 20kPa, see Fig. 1. Each combination of N and μ was run five times, starting from different initial random configurations. In each simulation, we varied μ in the range $[0.01, 10]$ for a total of 20 different assemblies. The pure shear, generated by the biaxial compression continued until, and beyond, the system reached a steady state of the global stress. We checked that, with one exception, which we discuss in detail below, no measurable quantity reached a steady state in any of the runs later than 8% strain. All data were collected at the steady state between strains of 8% and 16%.

B. Cells and cell stresses

A cell c is a polygon, whose vertices are the centroids of the overlapping areas of its surrounding grains, shown as the red shaded area in Fig. 2. These centroids are regarded as 'contact points'. The cell polygons in our simulations were generically convex, although this need not generally be the case [23]. The order of a cell, $k(\geq 3)$, is defined as the number of grains surrounding it. Our evaluation is limited to cells of order $k \leq 8$ in the absence of good statistics for the rare and short-lived higher order cells.

We also define the cell stress σ^c , based on the stresses of the grains surrounding it, as

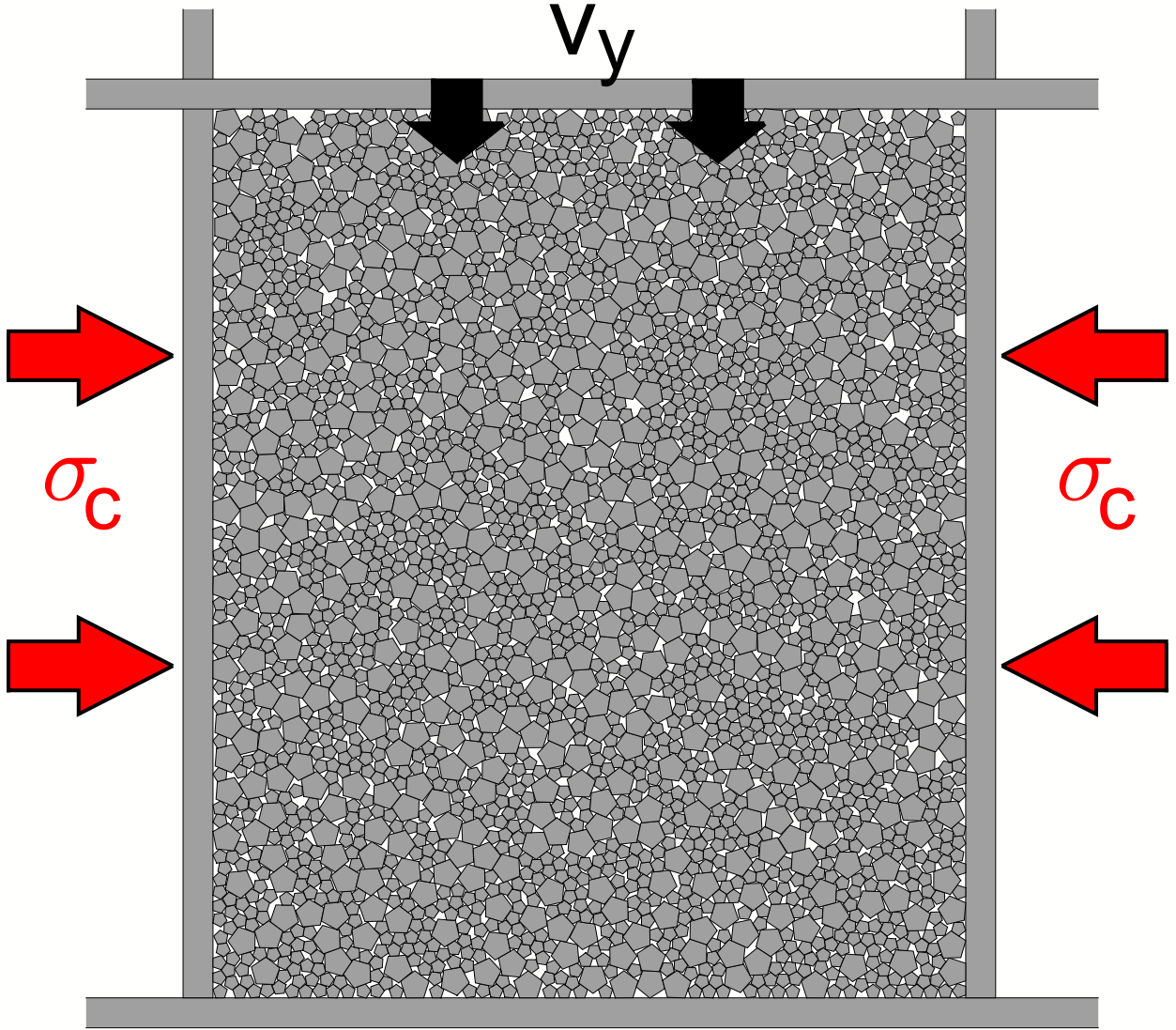


FIG. 1. The biaxial shear setup and boundary conditions. The top wall is lowered down at a constant speed v_y and the side walls are free to move to maintain a constant confining pressure σ_c .

follows. A grain stress is

$$\boldsymbol{\sigma}^p = \frac{1}{A^p} \sum_{p'} \mathbf{l}^{pp'} \otimes \mathbf{f}^{p'p}, \quad (1)$$

with p' the grains in contact with p , $\mathbf{l}^{p'p}$ vectors connecting the centre of p with the contact with p' , $\mathbf{f}^{p'p}$ the contact force between p and p' . The grain area, A^p , is the sum of the areas of its quadrans [24, 25]: A^{pc} , $A^{p'c}$, $A^{pc''}$, which extend to its surrounding cells, respectively,

c, c', c'' , as shown in Fig. 2. The cell stress is then defined as

$$\sigma^c = \frac{\sum_{p \in c} A^{pc} \sigma^p}{\sum_{p \in c} A^{pc}}, \quad (2)$$

with $p \in c$ denoting the polygons surrounding cell c .

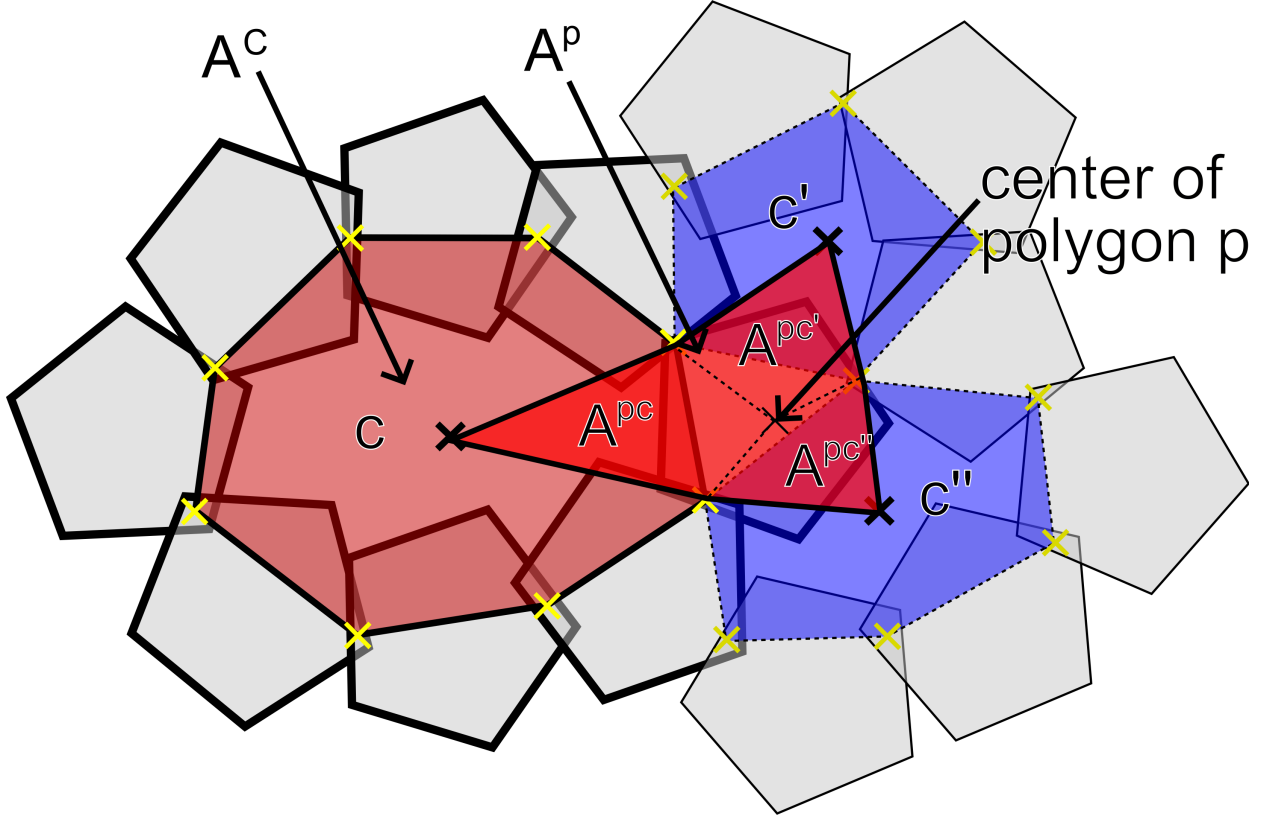


FIG. 2. An example of a cell of order $k = 8$: The cell is represented as a polygon, whose vertices are the centroids of the overlapping areas of its surrounding grains. A^{pc} , $A^{pc'}$, and $A^{pc''}$ are the areas of the quadrons of p extending into its surrounding cells, respectively, c , c' , and c'' . The cell area is the sum of the quadrons of the grains extending into it.

III. RESULTS

We find that the conditional cell order probabilities, $P(k|N)$, depend on on both the angularity and on friction (Fig. 3) – the more angular the grains the more sensitive they are to μ . Interestingly, while cells of order 3 are the most frequent for $N \leq 13$, cells of order 4 are the most frequent when N increases. As expected, increasing μ also increases

the occurrence probabilities of high-order cells, but up to cell order 5, $P(k \leq 5|N)$ decreases with μ for all N . Reducing N increases the proportion of order-3 cells and more compact structures. For high k , $P(k \leq 5|N)$ is found to depend somewhat on μ and hardly at all on N . The rates of merging and breaking of cells fluctuate about the steady-state values and these fluctuations increase with both μ and N (see Fig. 3 in the supplementary material (SM) [26]).

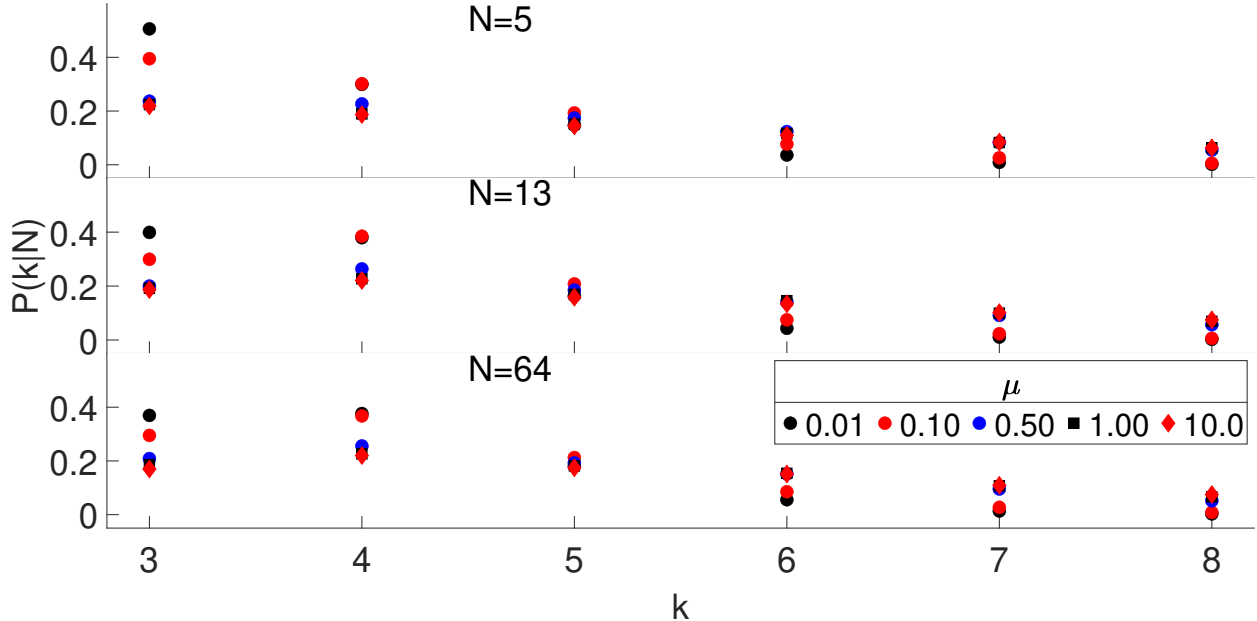


FIG. 3. The steady-state conditional probabilities $P(k|N)$ of the cell orders k for different angularities.

Denoting the principal cells stresses σ_1^c and $\sigma_2^c < \sigma_1^c$, $h = \sigma_2^c/\sigma_1^c$ is a measure of cell stability. The conditional probability density function (PDF) of h , $P(h|k)$, was found in [3] to collapse to a Weibull distribution in disc systems for all k and μ , when scaled by the mean \bar{h}_k , $P(\hat{h} \equiv h/\bar{h}_k|k) = P(\hat{h}) \forall k$. Scaling, for each value of μ , by $\bar{h}_k(\mu)$, find a good collapse for all k , shown in Fig. 4. Scaling by the average of $\bar{h}_k(\mu)$ over all values of μ yields a relatively good collapse for $N = 64$, but the collapse's quality deteriorates with angularity. These collapses are also fitted well by the Weibull form

$$P(\hat{h}) = \frac{m}{\lambda} \left(\frac{\hat{h}}{\lambda} \right)^{m-1} e^{-(\hat{h}/\lambda)^m}, \quad (3)$$

with m and λ hardly depending on N (see Fig. 4 in the SM [26]), $m = 3.1 \pm 0.1$ and $\lambda = 0.949 \pm 0.002$.

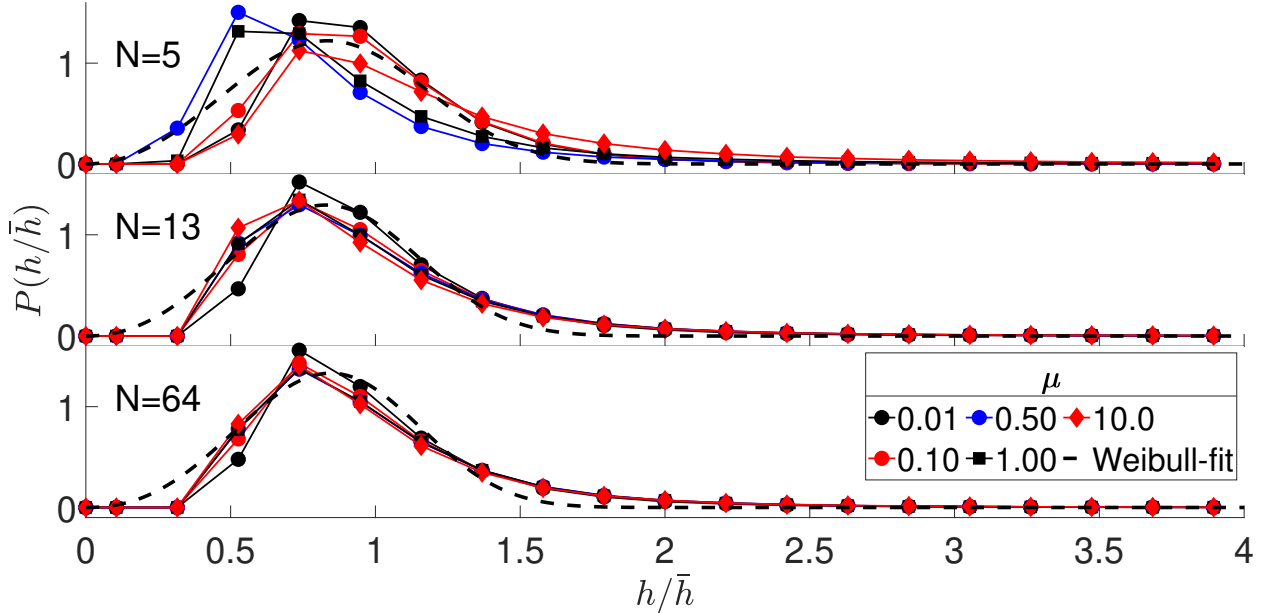


FIG. 4. The collapsed form of $P(\hat{h})$ for different values of μ and N . The dashed lines represent Weibull-distribution fits for the different values of μ .

In Fig. 5 we plot the mean cell stress ratio for each k , N , and μ . While the initial evolution of the cell stress-ratio, σ_1/σ_2 , is qualitatively different for the different combinations of N and μ , the steady-state values were very similar. This is further highlighted in Fig. 5 in the SM [26]. The exception from the above is the most angular grains assembly, $N = 5$, which we discuss in detail below and in the concluding section. Nevertheless, the convergence in almost all cases to a very similar steady-state stress ratio, observed here for the first time, supports further the idea of cooperative stress-structure self-organisation [3].

In Fig. 5 in the SM [26], we see that the steady-state values of \hat{h} first increase with μ and then decrease, with the decrease more pronounced with increasing angularity and almost disappearing for $N = 64$, when $k = 8$. We confirm earlier observations [19] that \hat{h} peaks at $\mu = 0.5$. This maximum is the result of two competing mechanisms, as we discuss in more detail below.

To investigate cell orientational organization, we approximate each cell as the ellipse closest to its contacts [3] (Fig. 6). We measured the ellipses' aspect ratios, α , and major axes orientations, θ^c . We omit in this analysis cells of order $k = 3$ for which the ellipse approximation is not useful. Figure 7 shows the evolution of α with strain for combinations of N and μ . At low friction, α is constant regardless of N . As μ increases the mean aspect

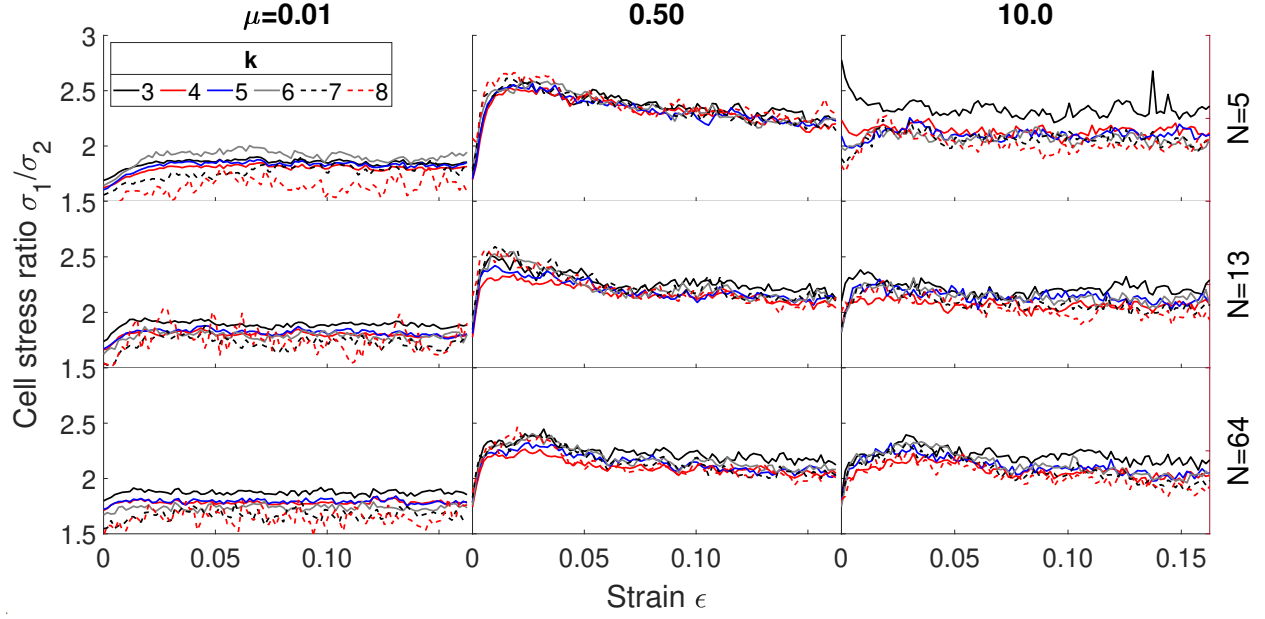


FIG. 5. Evolution of the mean cell stress ratio with strain for each order of cell and different combinations of μ and N .



FIG. 6. Example of ellipses fitted to the cells.

ratio increases and then decrease to a steady state value. The maximum is more pronounced for large k , low N , and high μ . It is hardly observable or disappears altogether for $k \leq 5$. In this regime, α decreases with increasing cell order. This can be understood in the context of

the entropy-mechanical stability competition [8], with the latter dominating at high-order cells.

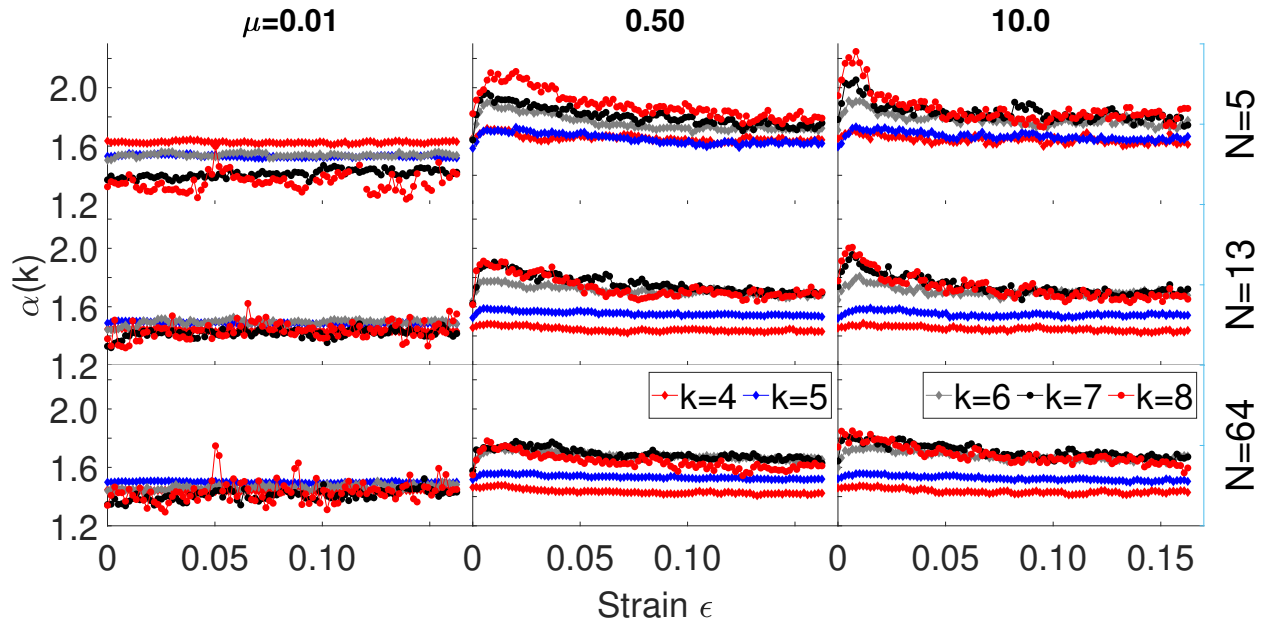


FIG. 7. Evolution of the mean cell aspect ratios. Cells of order $k = 3$ are excluded.

As expected, the steady-state value of α increases with μ for all $k > 4$ up to a value of μ in the range $[0.5, 1.0]$, which depends on the cell order. The rate of increase itself decreases with both N and k (Fig. 8). Higher friction enhances cells stability allowing more elongated cells to survive shear, an effect that is more pronounced for $k > 4$. High angularity also increases elongated cell stability owing to the hindered rearrangement of particles by rotation.

Cell organization is driven by stresses and we find that, for all N and μ , there is a strong correlation between cell orientations θ^c (see also Fig. 6 in the SM [26]) and the local major stress principal axis θ^S . In Fig. 9 we plot the distribution of the local difference between the two orientations, $\Delta\theta \equiv \theta^c - \theta^S$, which shows clearly their tendency to align. This phenomenon, which is more pronounced at high-order cells, is as in disc systems [2, 3], suggesting that it is independent of grain angularity.

We understand the dynamics that lead to such organisation as follows: Although the process is quasistatic, reorientation of cells requires unbalanced forces to move particles. This means that the cell stresses are momentarily asymmetric, giving rise to small torques that rotate them. The less stable the cell the larger the rotation. A measure of stability is the ratio of the mean shear stress, τ , and the trace, p , $\tau/p = (\sigma_1 - \sigma_2)F \sin(2\Delta\theta)/(\sigma_1 + \sigma_2)$.

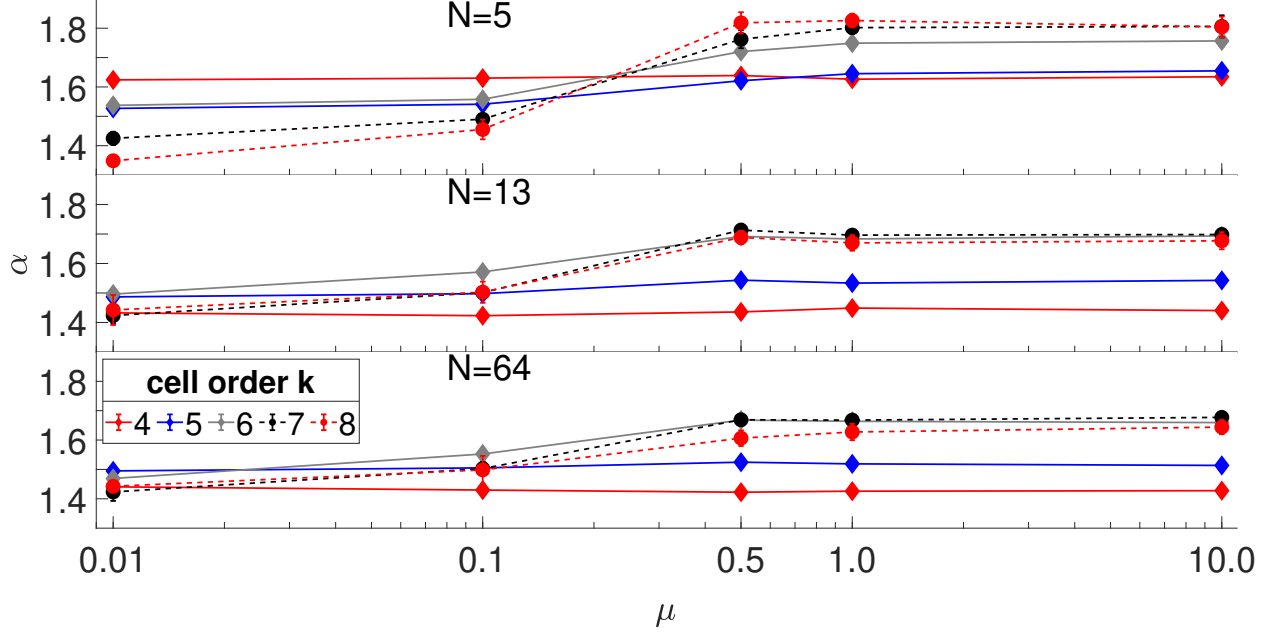


FIG. 8. Cell aspect ratios at steady state as a function of μ for different angularity N .

Thus, the nudging of the less stable cells towards higher stability during the process reduces $\Delta\theta$ and gives rise to the observed peak around $\Delta\theta = 0$. This can also be seen in the scatter plot of cells in the plane spanned by $\Delta\theta$ and τ/p , shown in Fig. 10.

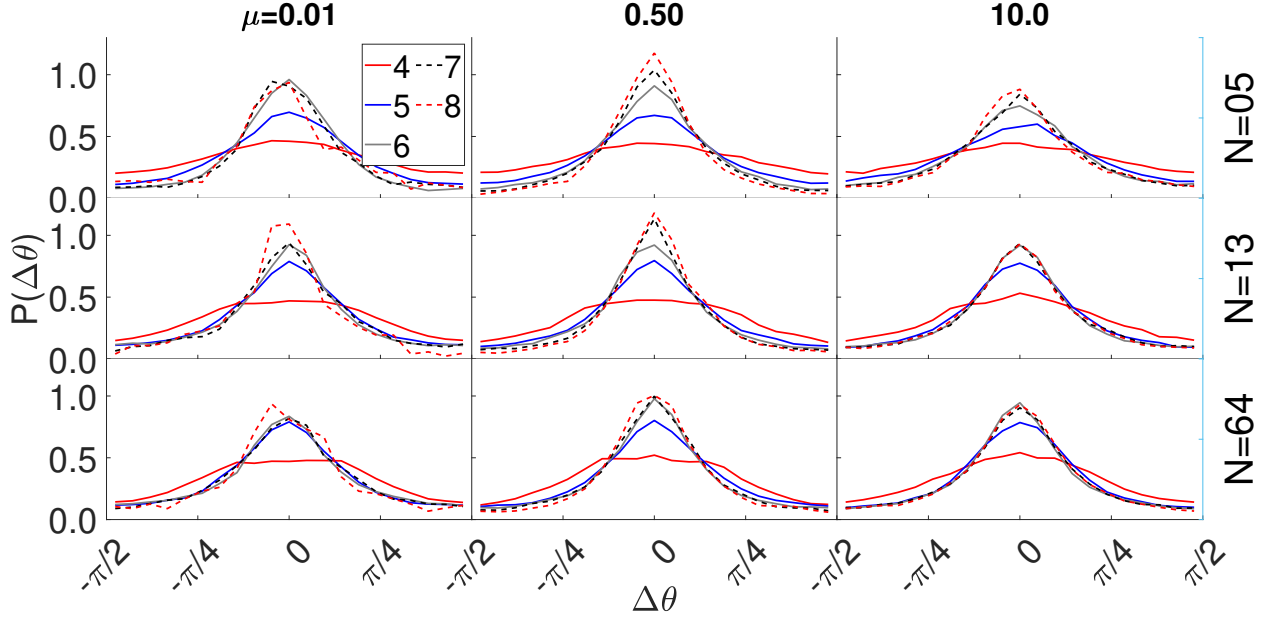


FIG. 9. PDF of $\Delta\theta \equiv \theta^c - \theta^S$ for different cell orders, k .

Overall, the behaviour of the most angular grain systems, $N = 5$, differs from the one

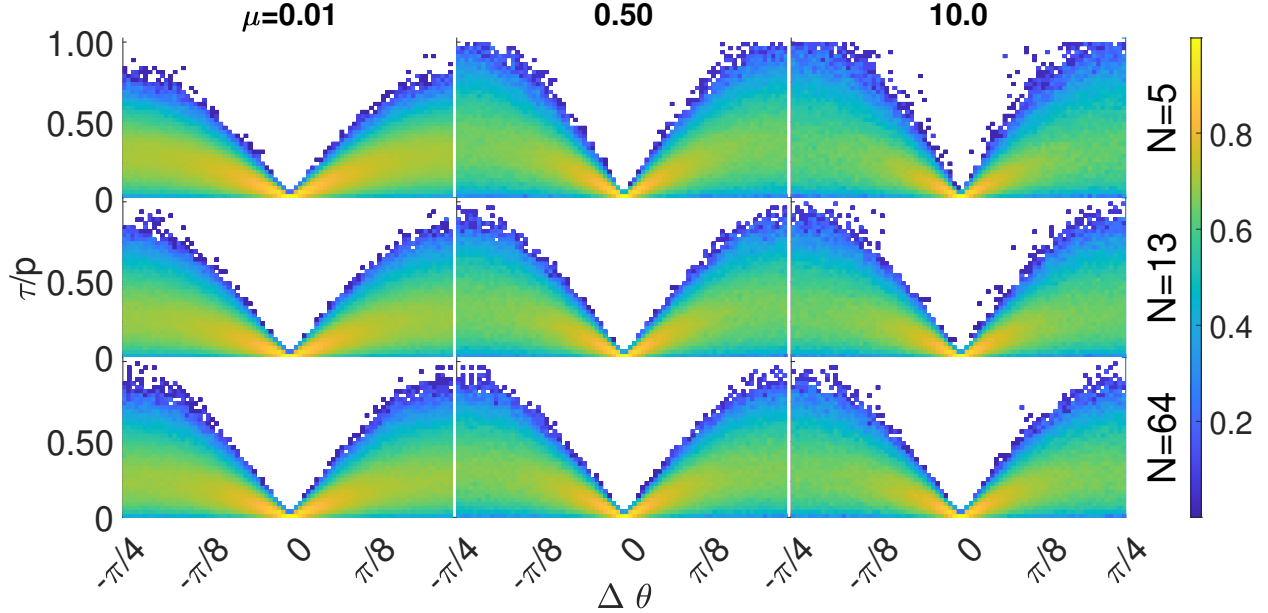


FIG. 10. A scatter plot heat map of cells in the plane spanned by $\Delta\theta$ and τ/p plane. The color denotes the relative frequency of cells with given values of $\Delta\theta$ and τ/p .

common to discs and high- N systems in several aspects, stemming from a competition between two cell rearrangement mechanism [19]: At low friction, while particle rearrangement is dominated by sliding, the surrounding granular matrix is easily deformable and particle rotation is induced by normal collisions. As the inter-particle friction increases, sliding across flat surfaces becomes increasingly restricted and frictional induced rotation starts to gain importance. However, for angular particles, the tangential force barrier to induce rotation is higher than for high- N particles, while at the same time larger contact interfaces dissipate more energy, so for a given value of μ contacts between angular particles are more stable than contacts between round particles. This in turn means, that higher order cells and larger cell aspect ratios are more likely for more angular grains.

IV. CONCLUSIONS

To conclude, we have studied the effects of grain angularity on self-organisation in quasi-static dynamics of 2D granular assemblies. We simulated regular polygonal grains with gradually sharper corners to test which of the indicators observed in disc systems survive increasing angularity. We have found that some indicators are independent of angularity

while others are not. Specifically, as in disc systems, individual cell stresses are well aligned with their orientations. Similarly, the PDFs of the scaled cell stress ratios, $P(\hat{h} = h/\bar{h}_k)$, collapse to a master Weibull form for all cell orders k . However, angularity affects the sensitivity of these PDFs to friction; as N decreases, the collapsed $P(\hat{h})$ appear to shift systematically toward lower values of \hat{h} as μ decreases. While one expects cells in low friction assemblies to be less stable, the reason for this difference is unclear. Since the angular corners are expected to have similar traction as in discs, we conjecture that the difference must stem from increased sensitivity to sliding of contacts between flat surfaces. It would be interesting to test this conjecture in future studies.

Another intriguing finding is that the steady-state behaviour changes around $\mu = 0.5$: the approach to steady state is slower (Fig. 5 in the SM [26]), there appears a peak in the mean ratio σ_1/σ_2 , and the resistance to shear increases. These phenomena become more noticeable with increasing angularity. These observations suggest an intricate competition between the sliding and rolling mechanisms that govern re-organisation. The probability of surface-to-surface contacts increases with angularity, increasing the sliding probability but reduces the rolling probability. As μ increases, the probability of rolling increases, but the barrier to rolling is higher for high-angularity grains. Nevertheless, once rolling takes place, the displacements of centers of high-angularity grains are larger. This competition gives rise to optimal stability at an intermediate value of μ , which happens to be around 0.5 in our bi-disperse polygonal systems.

ACKNOWLEDGMENTS

D. Krenzel, T. Matsushima and R. Blumenfeld are grateful for the support of the Grant-in-Aid for Scientific Research 21KK0071 from the Japan Society for the Promotion of Science (JSPS). D. Krenzel and T. Matsushima are further grateful for the support of the Grant-in-Aid for Scientific Research 21H01422 from JSPS.

SUPPLEMENTARY MATERIAL

V. SUPPLEMENTARY FIGURES

A. Visualization of the cells

In Fig. 11, the left panel shows examples of cells within the aggregates for different combinations of N and μ . When $\mu = 10.0$, angular particles readily form cells with $k > 8$. The particles within these cells are rattlers, as the superimposed force network (black lines) illustrates in the right panel.

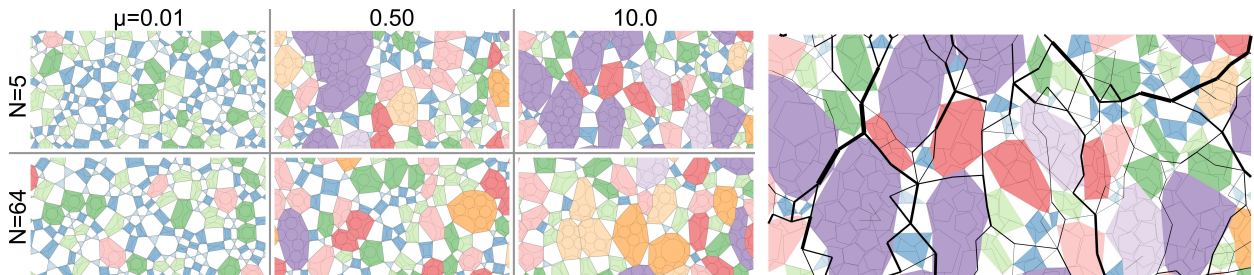


FIG. 11. (Left) Close-up view of steady-state cell structures of most and least angular particles when $\mu = 0.01, 0.50$, and 10.0 . Cells are coloured according to their order. The fraction of high-order cells increases both with angularity and friction. These cells contain more rattlers, as evidenced by the superimposed force chains (black lines) in the right panel for $N = 5, \mu = 10.0$.

B. The rate of change of $P(k|N)$

Fig. 12 illustrates the convergence of the cell conditional probability distributions to their steady-state values, $dP(k|N)/dt \rightarrow 0$, for different values of N and μ . The fluctuations around the steady state increase somewhat with μ , which is expected to be a general feature. In contrast, the difference between the initial convergence of the very low-friction systems ($\mu = 0.01$) and the other systems is attributed to the initial system preparation and the particular procedure we used to generate the steady state.

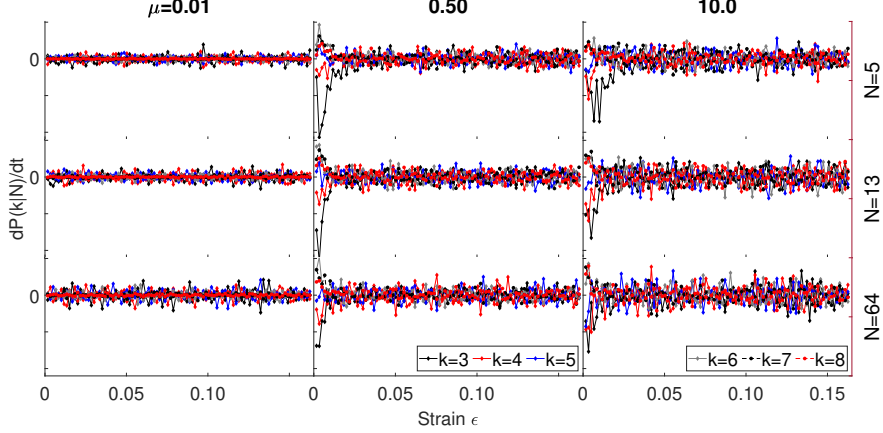


FIG. 12. The rate of change of the cell conditional probabilities, $dP(k|N)/dt$, with strain for different combinations of friction μ and angularity N .

C. N -dependence of the collapsed $P(\hat{h})$

The best fits for the order-independent collapse of the PDFs over different μ for any given N , have been shown in the main text to have the Weibull form,

$$P(\hat{h}) = \frac{m}{\lambda} \left(\frac{\hat{h}}{\lambda} \right)^{m-1} e^{-(\hat{h}/\lambda)^m}. \quad (4)$$

With the exception of hexagonal shapes ($N = 6$) the parameters m and λ are independent of N , as shown in Fig. 13. The PDFs $P(\hat{h})$ can also be approximated with a k-Gamma distribution,

$$P(\hat{h}) = \frac{\hat{h}^{k-1} e^{-(\hat{h}/\theta)}}{\theta^k \Gamma(k)}, \quad (5)$$

although the quality of each fit is notably worse than for the Weibull distribution, and the parameters no longer appear to be independent of N , but rather increase as N grows larger.

D. The μ -dependence of the steady-state stress ratio

The steady-state values of the stress ratio σ_1/σ_2 , shown in Fig. 5 of the main text, show a non-monotonic dependence on the inter-particle friction coefficient, see Fig. 14. We observe an increase in σ_1/σ_2 with μ until a maximum between $0.1 \leq \mu \leq 0.5$. For $\mu \geq 1.0$ the stress ratio decreases again, with the decrease appearing to depend on both cell order and particle shape. As explained in the main text, we understand the reason for this behaviour

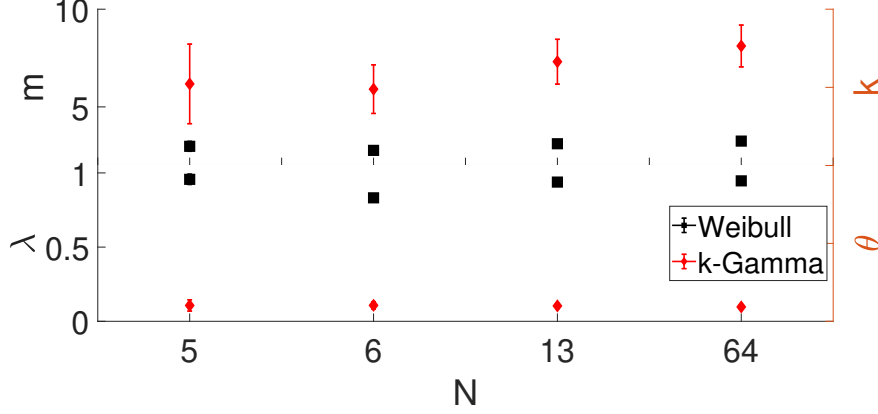


FIG. 13. N -dependence of the parameters of the Weibull distribution fit to the cell probability distributions in Fig. 4 in the main text. For reference we also plot the parameters of a k -Gamma distribution to the same data. The error for the Weibull parameters is too small to be seen at this scale.

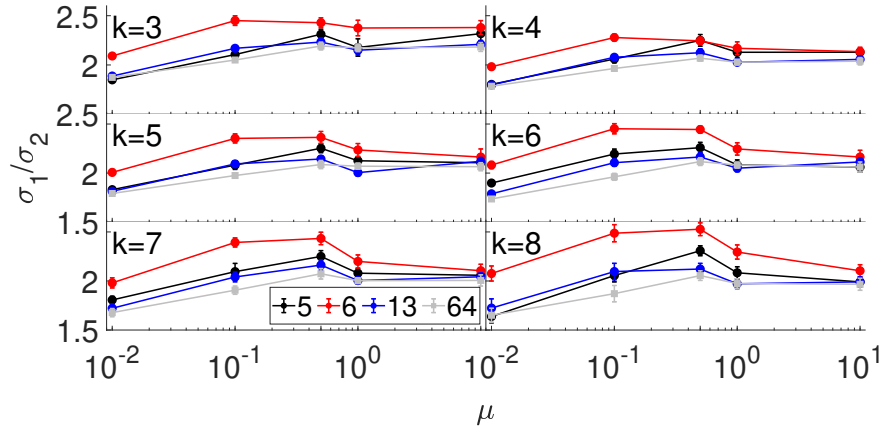


FIG. 14. Dependence of the steady state stresses ratio, shown in Fig. 5 in the main file, on μ and N .

as a competition between sliding and rolling that leads to an optimal stability at around $\mu = 0.5$.

E. Global cell orientation distribution

In Fig. 15, we plot the steady-state PDF of cell orientations for all $k > 3$. As expected, cells tend to align with the applied load, regardless of N . At low friction ($\mu \leq 0.1$), the PDFs approach the uniform form both because cells are less elongated and because the

media around cells are more mobile and therefore allow easier cell reorientation.

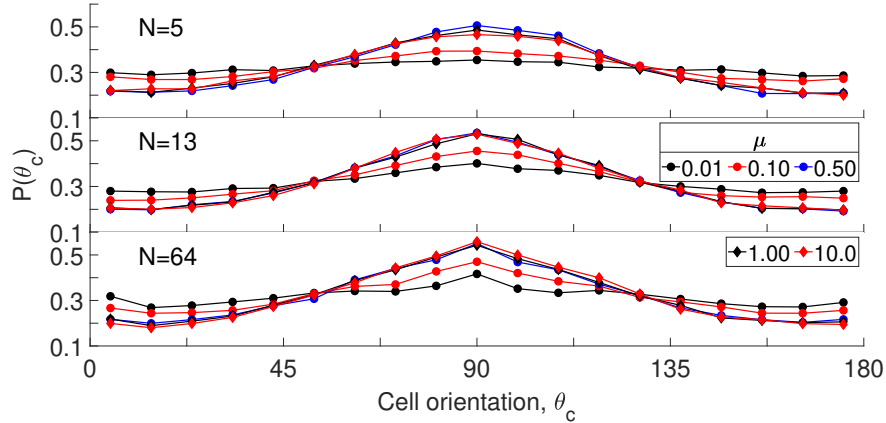


FIG. 15. Overall mean cell orientation, θ_c , relative to the horizontal direction, in the steady state.

-
- [1] T. Matsushima and R. Blumenfeld, Fundamental structural characteristics of planar granular assemblies: Self-organization and scaling away friction and initial state, *Physical Review E* **95**, 032905 (2017).
 - [2] T. Matsushima and R. Blumenfeld, Statistical properties of cell stresses in 2d granular solids, *EPJ Web of Conferences* **249**, 02006 (2021).
 - [3] X. Jiang, R. Blumenfeld, and T. Matsushima, Coordinated stress-structure self-organization in granular packings, *Physical Review E* **105**, 012901 (2022).
 - [4] N.-S. Nguyen, H. Magoaric, B. Cambou, and A. Danescu, Analysis of structure and strain at the meso-scale in 2d granular materials, *International Journal of Solids and Structures* **46**, 3257 (2009).
 - [5] H. Zhu, F. Nicot, and F. Darve, Meso-structure organization in two-dimensional granular materials along biaxial loading path, *International Journal of Solids and Structures* **96**, 25 (2016).
 - [6] H. Zhu, F. Nicot, and F. Darve, Meso-structure evolution in a 2d granular material during biaxial loading, *Granular Matter* **18**, 10.1007/s10035-016-0608-2 (2016).
 - [7] T. Matsushima and R. Blumenfeld, Universal structural characteristics of planar granular packs, *Physical Review Letters* **112**, 098003 (2014).

- [8] X. Sun, W. Kob, R. Blumenfeld, H. Tong, Y. Wang, and J. Zhang, Friction-controlled entropy-stability competition in granular systems, *Physical Review Letters* **125**, 268005 (2020).
- [9] C. C. Wanjura, P. Gago, T. Matsushima, and R. Blumenfeld, Structural evolution of granular systems: theory, *Granular Matter* **22**, 10.1007/s10035-020-01056-4 (2020).
- [10] X. Sun, Y. Wang, Y. Wang, R. Blumenfeld, and J. Zhang, Experimental evidence of detailed balance in granular systems, arXiv 10.48550/ARXIV.2105.01355 (2021).
- [11] A. D. C. Myhill and R. Blumenfeld, Steady states of two-dimensional granular systems are unique, stable, and sometimes satisfy detailed balance, *Journal of Physics A: Mathematical and Theoretical* **56**, 345001 (2023).
- [12] C. C. Wanjura, A. Mayländer, O. Marti, and R. Blumenfeld, Detailed balance in non-equilibrium dynamics of granular matter: derivation and implications, arXiv 10.48550/ARXIV.2404.05059 (2024).
- [13] E. Azéma, N. Estrada, and F. Radjaï, Nonlinear effects of particle shape angularity in sheared granular media, *Physical Review E* **86**, 041301 (2012).
- [14] D. Krenzel, J. Chen, and M. Kikumoto, Effects of particle angularity on the bulk-characteristics of granular assemblies under plane strain condition, *Computers and Geotechnics* **164**, 105812 (2023).
- [15] H. Jiang, R. Kawamoto, and M. Takashi, Coupled effects of particle shape and inter-particle friction on quasi-static shear behavior of dry granular materials studied by 2D LS-DEM, *Journal of Structural Engineering A* **70A**, 141 (2024).
- [16] Y. Hua, Y. Xin, H. Dai, H. Yang, Z. Chi, and R. Li, Study on the stability of particle packing structure based on cells, *Frontiers in Physics* **10**, 10.3389/fphy.2022.994121 (2022).
- [17] T. Binaree, E. Azéma, N. Estrada, M. Renouf, and I. Preechawuttipong, Combined effects of contact friction and particle shape on strength properties and microstructure of sheared granular media, *Physical Review E* **102**, 022901 (2020).
- [18] T. Binaree, E. Azéma, N. Estrada, M. Renouf, and I. Preechawuttipong, Shape or friction? which of these characteristics drives the shear strength in granular systems?, *EPJ Web of Conferences* **249**, 06008 (2021).
- [19] D. Krenzel, H. Jiang, J. Chen, and T. Matsushima, The combined effect of particle angularity and inter-particle friction on micro- and macroscopic properties of granular assemblies, *Computers and Geotechnics* **177**, 106850 (2025).

- [20] H. Jiang, *An LS-DEM Study on Contact-based Cell and Cluster Structures in Complex Granular Materials: From Static Packing to Dense Flow*, Ph.D. thesis, University of Tsukuba (2024).
- [21] X. Jiang, T. Matsushima, and R. Blumenfeld, Structural characteristics of ordered clusters in packs of ellipses, *EPJ Web of Conferences* **249**, 06004 (2021).
- [22] H. Matuttis and J. Chen, *Understanding the Discrete Element Method: Simulation of Non-Spherical Particles for Granular and Multi-body Systems*, 1st ed. (Wiley, Singapore, 2014).
- [23] Cell convexity is realised when surface 'point contacts' are defined as the middle points of the parts of the surfaces in contact.
- [24] R. Blumenfeld, Stresses in isostatic granular systems and emergence of force chains, *Physical Review Letters* **93**, 108301 (2004).
- [25] R. Blumenfeld and S. F. Edwards, Geometric partition functions of cellular systems: Explicit calculation of the entropy in two and three dimensions, *The European Physical Journal E* **19**, 23 (2006).
- [26] See supplemental material at [url-will-be-inserted-by-publisher] for visualization of the cells and complementary analysis not covered in the main text.